Coherent Wireless Link at 300 GHz With 160 Gbit/s Enabled by a Photonic Transmitter

Simon Nellen, Sebastian Lauck, Emilien Peytavit, Pascal Szriftgiser, *Senior Member, IEEE*, Martin Schell, *Member, IEEE*, Guillaume Ducournau, *Member, IEEE*, and Björn Globisch

***Abstract*—The increasing demand for high-capacity wireless communication requires data links at millimeter waves and terahertz frequencies, respectively. At those frequencies, electronic and photonic technologies compete to prove powerful transmitters and receivers. In this work, we demonstrate a wireless link at 300 GHz using a fiber-coupled PIN photodiode as the transmitter. Thus, the whole emitter side is based on components and techniques from standard fiber-optical communication, which inherently enable broadband data channels. We investigated two antenna designs with amplitude modulated and coherent data signals. Despite similar characteristics in terms of output power and carrier bandwidth, the quality of the data signals differed significantly. In addition, we found that the bit-error ratio (BER) scales non-monotonically with the optical input power of the photodiode, which is proportional to the terahertz output power. Depending on the modulation format and the symbol rate, we identified the optimal driving conditions of the photodiode. For amplitude modulation at 5 Gbit/s, we achieved error-free transmission with a BER of 7.5×10^{-13}. QPSK modulation was error-free up to 64 Gbit/s. The highest line rate of 160 Gbit/s was achieved with 32QAM modulation. This corresponds to 133 Gbit/s net data rate after forward-error correction with 20% overhead. The highest spectral efficiency was achieved with 64QAM at 8 GBaud, i.e., 48 Gbit/s line rate. The presented results highlight the high bandwidth of photonic wireless THz links. Furthermore, the carefully analysis helps to improve the quality of future wireless links in the 300 GHz band.**

***Index Terms*—300 GHz link, optoelectronic emitter, photonic transmitter, terahertz communication, wireless link.**

I. Introduction

DUE to the steadily increasing demand for high-speed wireless data transmission, R&D groups around the world target higher carrier frequencies, up to the terahertz range (0.1 THz to 10 THz), in order to increase the bandwidth of transmission channels [1]–[7]. Latest research mainly focused on carrier frequencies around 300 GHz, due to the atmospheric transmission window in this frequency range [8]. Additionally, frequencies up to 320 GHz have been standardized already by IEEE 802.15.3d [9]. In this application, optoelectronic devices have considerable advantages compared to all-electronic systems: first, the high bandwidth of optoelectronic emitter and receiver devices can cover broad transmission channels. Second, the incoming data stream from a fiber-optical network can be directly modulated on a terahertz carrier wave without conversion into the baseband. Third, carrier frequencies above 300 GHz can be addressed without the need to develop fundamental new hardware.

High-speed photodiodes (PDs), originally developed as detectors in fiber-optical communication networks, are commonly employed as emitters in optoelectronic terahertz spectrometers. The principle of operation is as follows: An optical beat signal is generated by the superposition of two lasers, which illuminates the PD emitter and generates a photocurrent with the difference frequency of the two lasers. If an antenna is attached to the PD, this modulated current can be radiated into free-space. Today, there are mainly two ways to radiate the terahertz signal from the PD into air: i) electrical coupling into a hollow waveguide for microwaves and horn antenna, respectively, or ii) quasi-optical coupling employing a substrate lens [10]. On the one hand, microwave waveguides are a widespread standard and allow the use of compatible electronic components, i.e., amplifiers and antennas to increase the emitter gain. On the other hand, the dimension of a hollow waveguide limits the transmission bandwidth. Typically, the available bandwidth of rectangular waveguides is about ±20% around the center frequency. Hence, the frequency range of the WR-3 waveguide is 220 GHz to 330 GHz according to the EIA band designation [11], [12]. The

Manuscript received November 7, 2021; revised January 26, 2022; accepted March 4, 2022. Date of publication March 22, 2022; date of current version July 2, 2022. This work was supported in part by TERAWAY Project that has received funding from the European Union's Horizon 2020 Research and Innovation Programme under Grant 871668 and it is an initiative of the Photonics Public Private Partnership, in part by the Bundesministerium für Bildung und Forschung (BMBF) through Project PHONOGRAPH under Grant 16KIS0638, in part by the ANR-DFG TERASONIC Grant, CPER Photonics for Society and WAVETECH @ HdF that supported the datacom setups used for terahertz links performance investigation, in part by DYDICO cluster of the I-site ULNE, in part by ITN TERAOPTICS, that has received funding from the European Union's Horizon 2020 Research and Innovation Programme under the Marie Skłodowska-Curie Grant 956857, in part by the ANR SPATIOTERA Project and TERIL-WAVES Project, funded by Metropole Européenne de Lille (MEL) and I-site ULNE by using a terahertz receiver that was developed within these projects, and the overall work is part of the IEMN UHD Flagship. IEMN also thanks the PCMP, CHOP (RF Characterization and Optics) platforms.

Simon Nellen and Sebastian Lauck are with the Fraunhofer Institute for Telecommunications, Heinrich Hertz Institute, 10587 Berlin, Germany (e-mail: simon.nellen@hhi.fraunhofer.de; sebastian.lauck@hhi.fraunhofer.de).

Emilien Peytavit and Guillaume Ducournau are with the Université de Lille, CNRS, Université Polytechnique Hauts-de-France, UMR 8520 - IEMN, F-59000 Lille, France (e-mail: emilien.peytavit@iemn.fr; guillaume.ducournau@univ-lille.fr).

Pascal Szriftgiser is with the Laboratoire de Physique des Lasers Atomes et Molécules (PhLAM), UMR CNRS 8523, Université Lille, F-59655 Villeneuve d'Ascq Cedex, France (e-mail: pascal.szriftgiser@univ-lille.fr).

Martin Schell and Björn Globisch are with the Fraunhofer Institute for Telecommunications, Heinrich Hertz Institute, 10587 Berlin, Germany, and also with the Technische Universität Berlin, Institut für Festkörperphysik, 10623 Berlin, Germany (e-mail: martin.schell@hhi.fraunhofer.de; bjoern.globisch@hhi.fraunhofer.de).

Color versions of one or more figures in this article are available at https://doi.org/10.1109/JLT.2022.3160096.

Digital Object Identifier 10.1109/JLT.2022.3160096

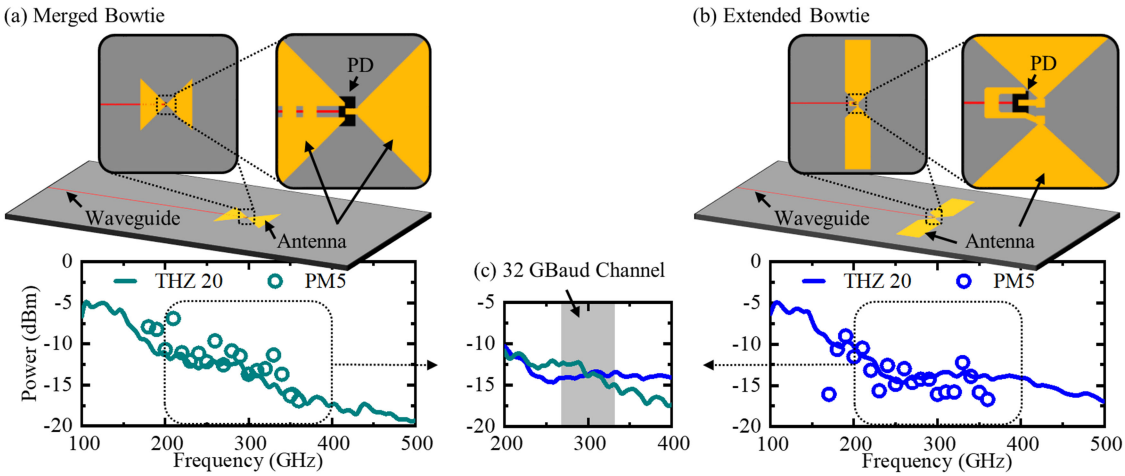

Fig. 1. Output power of a fiber-coupled, substrate-lens mounted emitter module with merged bowtie (a) and state-of-the-art extended bowtie design (b). The terahertz power was measured with two different power meters: i) a pyroelectric free-space detector (THZ 20) for frequencies of 100 GHz - 500 GHz (full line) and ii) a power detector with horn antenna (PM5) for frequencies of 170 GHz - 360 GHz (open circles). The optical power fed into the PD was a 15 dBm unmodulated beat note signal around 1550 nm. The upper part of subplot (a) and (b) illustrates the respective antenna chip (1.5 mm $\times$ 3.0 mm) with optical waveguide, feeding point structure and antenna. The direct comparison of curves measured with the THZ 20 detector (c) reveals a flat response of the extended bowtie around 300 GHz, whereas $\sim$3 dB power variation are observed across a 32 GBaud channel for the merged design bowtie.

quasi-optical approach, however, is not fundamentally limited in bandwidth, but is expected to have a flat transfer function as long as the material is translucent for the frequency. Thus, this approach is chosen in the present work to exploit both the high carrier and channel bandwidth of an optoelectronic terahertz link. Note that the frequency response of the photodiode mainly determines the frequency response of the emitter since bowtie antenna and quasi-optical coupling are spectrally flat in principle. However, two types of photodiodes can be found in today's terahertz emitters: unitraveling-carrier photodiodes (UTC-PD) and positive-intrinsic-negative photodiodes (PIN-PD). The respective carrier dynamics of those types of PDs is different, whereas the concept of terahertz frequency generation is identical. A detailed description and comparison of UTC- and PIN-PD-based terahertz emitters can be found in [13]. However, the fabrication of PIN-PDs is based on mature processes originally developed for fiber optical communication systems and PIN-PDs have been used as broadband terahertz emitters for spectroscopy for more than 10 years [14]. Thus, we used a PIN-PD-based emitter in this work.

In previous work, we already reported on a 100 Gbit/s net data rate at 300 GHz carrier frequency based on a PIN-PD emitter in combination with an electronic I/Q receiver, i.e., direct demodulation to in-phase and quadrature (I/Q) components of the signal [5]. Fully optoelectronic links employing a PIN-PD emitter and photoconductive antennas as receiver demonstrated the high range of accessible carrier frequencies of optoelectronics [6], [15]. The PIN-PD emitters we used in those experiments were originally developed for terahertz spectroscopy instead of wireless communication. However, the demands on terahertz emitters for these two applications are essentially different. In wireless communication, the beam profile is highly relevant because no additional beam forming or guiding elements can be used at any point of the free-space link. Therefore, we investigated the radiation pattern of state-of-the-art PIN-PD emitters [16] and compared it to alternative antenna designs [14]. In [14], we reported on reduced unwanted side lobes in the radiation pattern of this new antenna design, which should help to avoid multi-path interference in a communication link. In addition, we expect an improved signal integrity of this new emitter design due to an improved feeding point structure. In order to verify this thesis in the present paper, we compare two antenna designs in a wireless communication link with carrier frequencies around 300 GHz. We demonstrate that the improved emitter enables gross data rates of 160 GBit/s at 32 GBaud on a single channel. To the best of our knowledge this is the highest data rate reported for a single channel around 300 GHz so far.

II. Measurements and Results

A. Power Characterization and Experimental Setup

Fig. 1 shows the antenna design and the power spectrum of the two different PD emitters investigated in this work. We restrict our analysis to these two types as they are the most promising designs from previous studies [14]. The upper part of each subplot depicts the indium phosphide (InP) chip with the optical waveguide and the metallic bowtie (BT) antenna. In both cases, the chip dimensions are 1.5 mm $\times$ 3.0 mm. The augmented view shows the feeding point of the device, i.e., the structure that connects the PD with the antenna. The extended bowtie (b) corresponds to BT#1 in reference [14] and represents the state-of-the-art PD emitter, which is commonly used for terahertz spectroscopy. The merged bowtie (a) corresponds to BT#3 in reference [14], which is the new design with an improved beam profile. In this work, we investigate, which of these designs is better suited for data transmission at 300 GHz. At this frequency, the radiation pattern of these antennas differs regarding width of the main lobe and intensity of side lobes: the 6dB beam angle is reported as $\pm 14°$ and $\pm 9°$, and the intensity of the side lobes as -2 dB and -13 dB for BT#1 and BT#3,

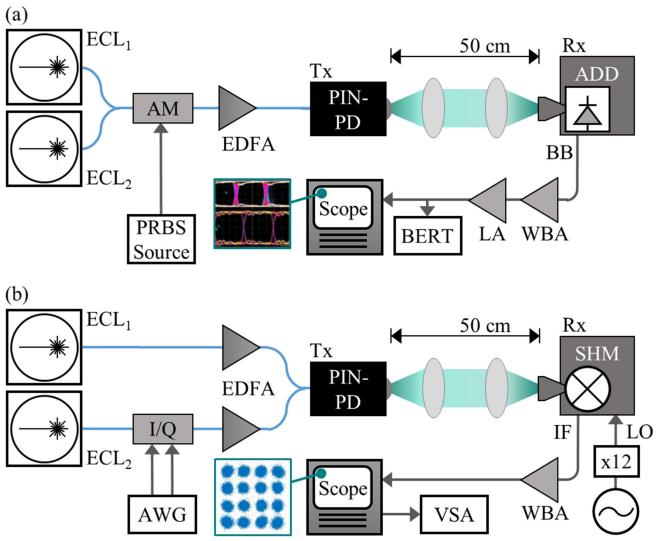

Fig. 2. Setup for 300 GHz communication: for NRZ-OOK (a), two external cavity lasers (ECL) with a frequency spacing of 300 GHz are combined in an optical fiber and fed into an amplitude modulator (AM). The modulator receives the data from a pseudo-random binary sequence (PRBS) generator. An erbium-doped fiber amplifier (EDFA) increases the optical signal before the emitter (Tx) converts the optical beat signal to 300 GHz radiation. For coherent data transmission (b), only the signal from ECL_2 is modulated in phase and amplitude (I/Q). An arbitrary waveform generator (AWG) drives the modulator. After amplification (EDFA) the signal from both ECLs are combined and fed into the Tx. Two HDPE lenses collimate and focus the beam to the receiver (Rx). To down-convert the NRZ-OOK signal (a) to base band (BB), the Rx is an amplified direct detector (ADD). For coherent detection (b), a subharmonic mixer (SHM) enables the conversion of data signals towards an intermediate frequency (IF) around 20 GHz. To generate a 150 GHz local oscillator (LO), the 12.5 GHz signal from a frequency synthesizer is multiplied by 12. A wideband amplifier (WBA) amplifies IF signal of the respective Rx. For NRZ-OOK (a), an additional limiting amplifier (LA) is used before analysis of the received data with a bit-error ratio tester (BERT) and equivalent time oscilloscope. For coherent data (b), a real-time oscilloscope samples the received data for I/Q analysis via the VSA software.

respectively [14]. The layer structure of the PD itself is identical to the PD reported in reference [13]. Fig. 1 also shows a power spectrum of a fiber-coupled emitter module. Two different types of power detectors have been used to characterize the terahertz output of the emitters: first, a calibrated pyroelectric power detector (THZ 20 from SLT, solid line), which measures in a free-space arrangement like in reference [13]. Second, a horn-coupled power detector (PM5 from Erickson, circles), which measures the unmodulated carrier signal in the setup that is later used for wireless communication by replacing the receiver (cf. Fig. 2). For the power characterization, the emitters were driven with 15 dBm optical power. Having in mind that power measurements in the terahertz frequency range are very sensitive to alignment, the presented results measured with two different power meters in two different setups are very comparable [17]. Both power measurements show the typical frequency response of the respective antenna structure around 300 GHz: i) the output power of the extended bowtie (b) is flat between 250 GHz and 350 GHz because of good impedance matching of PD and antenna. This is due to the feeding point structure of this device. Details can be found in [14]. ii) For the merged bowtie (a), the continuous roll-off toward higher frequencies without plateaus is caused by a reduced feeding point structure, which does not allow for impedance matching [14].

The flat response of the extended bowtie (b) within the dedicated communication frequency range around 300 GHz is expected to result in less signal distortion especially for high channel bandwidth. The merged bowtie, on the other hand, should provide higher signal integrity due to the reduced side lobes in the radiation pattern and the increased signal integrity of the merged feeding point. The direct comparison of the spectral output power in a 32 GBaud channel around 300 GHz (gray area in Fig. 1(c)) shows 3 dB variation in case of the merged bowtie, but only 1.2 dB for the extended bowtie. Thus, the two types of antenna design represent the trade-off between signal integrity and channel flatness. In order to investigate the influence of that trade-off to the capability of a terahertz link, we compared both types of antenna in an amplitude modulation testbed. Afterward, the merged bowtie antenna was also employed as an emitter in a coherent 300 GHz link.

Fig. 2 illustrates the experimental testbed for two communication schemes: (a) non-return-to-zero (NRZ) on-off-keying (OOK) and (b) coherent (I/Q) quadrature-amplitude-modulation (QAM). For OOK (Fig. 2(a)) two external cavity lasers (ECL, instantaneous linewidth around 100 kHz) operating in the optical C-band were set to $\sim$300 GHz frequency separation. After superposition in an optical fiber, an amplitude modulator (AM) modulated the data signal from a pseudo-random binary sequence (PRBS) generator to the optical beat signal. The used Mach-Zehnder modulator has a 40 Gbit/s baseband performance. After that, an erbium-doped fiber amplifier (EDFA) boosted the optical signal to the desired power level before it was fed into the emitter (Tx). Two lenses focused the 300 GHz signal into the horn antenna of the receiver (Rx) in a distance of 50 cm. The lenses are made from ZEONEX material, with a diameter of 25 mm and a focal length of 25 mm. Thus, an effective beam angle of $\pm 26.5\,^{\circ}$ of the emitter is used for the data transmission, which is sufficient to include the emitter's main lobe down to approx. -20 dB [14]. In order to receive the NRZ-OOK signals, an amplified direct detector (ADD) was used. The ADD is composed of two core components: (i) a III-V amplifier with 25 dB gain, 12 dB noise figure and $>$ 50 GHz bandwidth around 300 GHz, and (ii) a GaAs Schottky diode featuring a high sensitivity of 1000 V/W at 300 GHz. The resulting intermediate frequency (IF) was post-amplified using a wideband amplifier (WBA) with 29 dB gain (SHF810 from SHF Communication Technologies AG) that allows detection of amplitude-modulated signals up to 25 Gbit/s. In order to properly drive the real-time bit error counting circuits, a limiting amplifier (LA) with additional 29 dB gain (Hittite evaluation board, HMC866) was also used for amplitude modulation [18]. Finally, a real-time bit-error ratio tester (BERT) measures the number of transmitted bit-errors.

Fig. 2(b) shows the arrangement for coherent data transmission. Here, we used a pair of ECLs with reduced linewidth of 10 kHz only in order to improve the purity of the optical data signal for coherent transmission. The first ECL remained unmodulated to act as the photonic local oscillator (PLO) to beat with the optical data signal. The output of the second ECL received the coherent data from an I/Q modulator that was

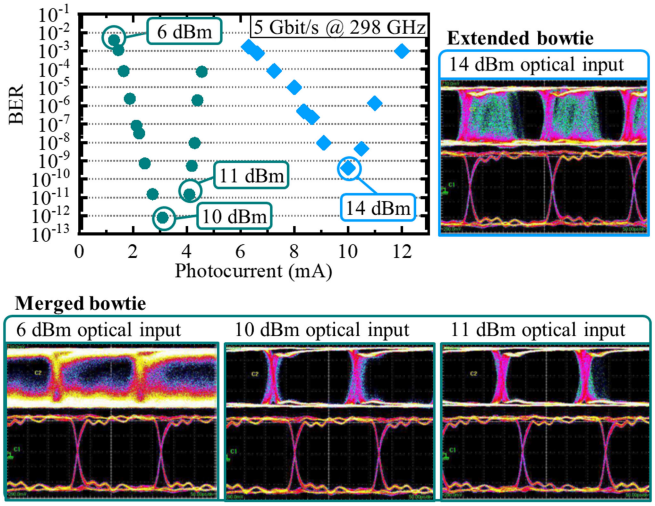

Fig. 3. The bit-error ratio (BER) for 5 Gbit/s as a function of photocurrent for the merged and extended bowtie antenna. The noise slopes lead to increasing BER beyond the respective sweet spot. In case of the extended bowtie, echoes, which are attributed to the antenna structure, results in closed eyes and thus higher BER.

controlled with an arbitrary waveform generator (AWG). Two EDFAs amplified modulated and unmodulated optical signals, respectively, before superposition to an optical beat signal. Thus, the power levels of the two optical tones could be controlled and the overall optical power fed into the PIN-PD could be set. In order to receive the coherent data, a subharmonic mixer (SHM), which is based on a GaAs diode with a subharmonic factor of 2, down-converted the 300 GHz signal to an IF around 20 GHz. In detail, the SHM was mixing the incoming 300 GHz signal with electronic local oscillator (LO) with a frequency of 150 GHz and an RF (radio frequency) power of 2 mW. The LO was created by driving a frequency multiplier chain (12-times) with a microwave synthesizer (12.5 GHz). With this 150 GHz LO, the conversion losses are 8 to 9 dB around 300 GHz with ±25 GHz RF bandwidth. The down-converted IF signal was amplified using the SHF810. Finally, the IF was fed to a wideband oscilloscope (UXR Keysight, 70 GHz) that was connected to the I/Q analysis tool (VSA from Keysight) [19]. The measurements were equalized to compensate the overall link linear distortion.

B. Amplitude Modulation and Influence of Antenna Design

Fig. 3 shows the bit-error ratio (BER) as a function of photocurrent for both emitters, i.e., the merged (green) and the extended (blue) bowtie. Various data rates were tested and all showed a non-monotonic dependence of the BER on the photocurrent. For a detailed comparison, we choose OOK with 5 Gbit/s data rate, since the particular noise behavior of the respective antenna emerges very clear. In case of the merged bowtie, a BER below 10^{-2} was achieved for photocurrents below 2 mA. The respective eye pattern shows a noise-dominated transmission: the optical reference signal (lower eye diagram) is clear, whereas the terahertz signal (upper eye diagram) is barely open with poor signal to noise ratio (SNR). With higher photocurrent, i.e., increased optical and hence increased terahertz power, the BER decreases and reaches its minimum of 7.5×10^{-13} at 3 mA photocurrent. At this point, the eyes are open with still noisy slopes. Surprisingly, for higher photocurrent the BER starts to increase again, however, with a different slope than for photocurrents below 3 mA. In contrast, the emitter with extended bowtie (blue) required more than 6 mA photocurrent for a BER below 10^{-2}. For higher photocurrents, this emitter shows a similar behavior as the merged bowtie. The BER decreases and reaches its minimum of 4×10^{-10} at 10 mA photocurrent, which corresponds to an optical illumination with 14 dBm. However, the eye diagram of the transmitted signal shows noisy slopes and significant echo features as vertical lines. In analogy to the merged bowtie emitter, higher photocurrents increase the BER as the echoes become more intense. For data rates higher than 5 GBit/s, we observed that the echoes fill the eye in the time domain and merge with subsequent bits. In summary, we observe a v-shaped BER curve with a pronounced minimum for both emitters. We attribute the left slope of the v-shaped BER to noise limitation, whereas the right slope of the BER curve is caused by increasing echoes and reflections. The origin of these echoes is not fully understood. We are currently performing numerical simulations to investigate this in detail. However, the only difference between the two emitters is the design of the feeding point and the bowtie antenna since the experimental setup (cf. Fig. 2(a)) and the packaging of the respective antenna chips were identical. One promising candidate, which might be responsible for causing echoes, is the impedance matching circuit between PD and antenna in the extended bowtie configuration (cf. Fig. 1). This design is applied to maximize the terahertz output around 300 GHz. As the extended bowtie shows pronounced echoes, this impedance matching circuit seems to have a detrimental effect on the signal integrity in wireless communication links. Hence, we restrict our subsequent experiments to the merged bowtie emitter.

The results presented in the OOK link also show that the lowest BER was measured for optical input powers below the maximum of 15 dBm. Thus, we investigate the dependence of the photocurrent and the terahertz output power at 300 GHz as a function of the optical illumination in Fig. 4. Assuming a constant responsivity (0.32 A/W), the photocurrent $\mathrm{I_{PD}}$ increases linearly with the optical power $\mathrm{P_{opt}}$. For optical power given in units of dBm, a logarithmic current scale (log A) results in a linear curve:

$$I_{PD}^{A} \propto P_{opt}^{W} \rightarrow I_{PD}^{\log(A)} \propto P_{opt}^{dBm} \tag{1}$$

The measured photocurrent (green circles in Fig. 4(a)) deviates from the line of constant responsivity (blue dashed line), when the photodiode starts to saturate regarding the optical input power. This occurs for 14 dBm optical power, which corresponds to a photocurrent of 7.3 mA. For the RF output power $\mathrm{P_{RF}}$ of the antenna, we assume a quadratic dependence on the RF current of the photodiode $\mathrm{I_{RF}}$. In an unsaturated regime, the RF current

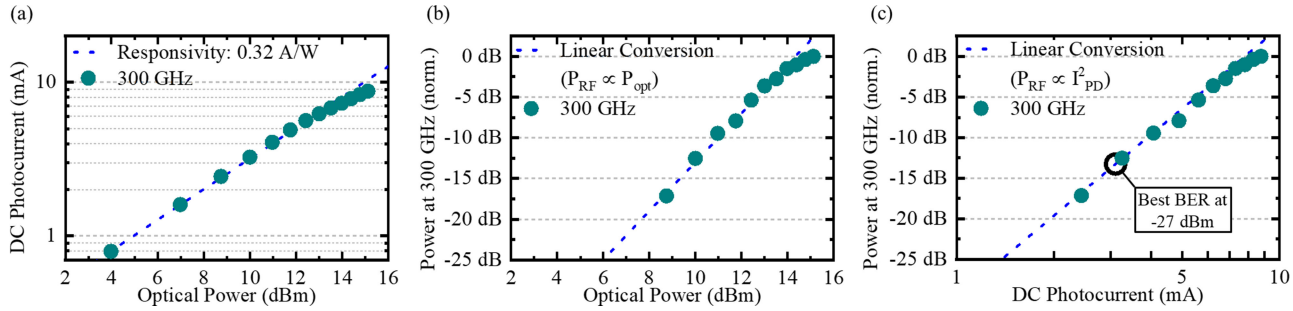

Fig. 4. Investigation of the terahertz emitter regarding linearity: photocurrent (a) and output power at 300 GHz (b) as a function of optical input power up to 15 dBm. (c) Shows the output power as a function of the photocurrent, since BER curves refer to photocurrent. At 14 dBm, the photocurrent (a) is no longer linear to the optical input power. The output power also shows the saturation at 14 dBm (b) or 7.3 mA (c), respectively. The output power is normalized to the value at 15 dBm optical input, i.e., recommended operation for commercial PIN-PD emitters. Considering the power spectra of Fig. 1, the absolute power required for lowest BER in 5 Gbit/s NRZ-OOK link is -27 dBm.

is proportional to the measured DC current I_{PD} [20]:

$$P_{RF} \propto I_{RF}^2 \propto I_{PD}^2 \tag{2}$$

Taking the proportionality between photocurrent and optical power into account, the conversion of optical input to RF output power is $P_{RF}^W \propto {I^2}_{PD}^A \propto P_{opt}^W$ or in logarithmic units

$$P_{RF}^{dB} \propto I_{PD}^{\log(A)} \propto P_{opt}^{dBm}. \tag{3}$$

Fig. 4(b) and (c) show the expected linear conversion as a function of optical power and photocurrent, respectively. Note that the graph in Fig. 4(b) is normalized to the output at 15 dBm optical power. In agreement with the derived relation between optical power, photocurrent and RF power, the saturation of the photocurrent (Fig. 4(a)) translates into a saturation of the output power at 300 GHz at 14 dBm optical power in Fig. 4(b) and at 7.3 mA photocurrent in (c). Hence, the results in Fig. 4 show that the terahertz output starts to saturate for photocurrents above 7.3 mA. Thus, the minimal BER of the merged bowtie, which was found at a photocurrent around 3 mA (cf. Fig. 3), cannot be explained by the onset of saturation of the terahertz output for this antenna.

C. Coherent Terahertz Link

Due to the higher signal integrity and the promising results in the OOK testbed, we employ the emitter with merged bowtie antenna in a coherent terahertz link (cf. Fig. 2(b)).

In analogy to the previous section, we investigate the BER as a function of photocurrent for different symbol rates and modulation formats. Fig. 5(a), (b) and (c) show the BER as a function of the photocurrent for symbol rates of 8 GBaud, 25 GBaud and 32 GBaud, respectively. For each symbol rate, the transmission with QPSK (quadrature phase-shift keying, i.e., 4QAM) data was quasi error-free, i.e., no error-bit was detected within 100000 transmitted symbols. Therefore, carrier recovery and equalization in the VSA were the only post-processing steps used for constellation analysis. In future terahertz links, such simple processes could be integrated in advanced ASICs (application-specific integrated circuit) or FPGAs (field-programmable gate array) as in optical coherent receivers. Note that the absolute values of BER for coherent transmission are orders of magnitude higher compared to amplitude modulation. This is mainly because amplitude modulation is associated with real-time BER measurements and does not include any signal processing steps. Thus, the detection is more sensitive to the frequency response of emitter, detector, and post-amplifiers. Nevertheless, in order to benefit from the high data rates of coherent modulation schemes, the additional effort of digital signal processing (DSP) is reasonable, although at the cost of non-real-time operation. In any case, we can note that all data points in Fig. 5 can be considered error-free after DSP when a soft-decision (SD) forward-error correction (FEC) with 20% overhead is used as the SD-FEC threshold is 2.2×10^{-2}.

At 8 GBaud (Fig. 5(a)), the BER shows the strongest dependence on the photocurrent. With 16QAM modulation, the BER drops to 8.8×10^{-7} when the photocurrent is increased to 4 mA. Beyond this photocurrent, the BER increases again. 32QAM modulation requires 4.5 mA photocurrent to reach the minimum BER of 2.9×10^{-4}. With the same photocurrent, 64QAM signals are transmitted with a BER of 5.4×10^{-3}, which is still well below the FEC threshold. However, for further increased photocurrent, the BER increases for all modulation formats except for QPSK, which remains error-free. Hence, the v-shape of the BER curves, which was already observed in our OOK measurements, also appears for coherent data links. For higher symbol rates, the v-shape of the BER curve can be clearly seen in Fig. 5(b) and (c) for 16QAM and 32QAM. However, the required photocurrent to achieve the lowest BER increases as the symbol rate increases. Hence, the trade-off between the reduction of noise by increasing the photocurrent and the reduction of unwanted echoes by decreasing the photocurrent seems to shift to higher photocurrents for higher symbol rates. In addition, the absolute value of the BER increases for higher symbol rates. In analogy to the OOK measurements, we attribute the increasing BER in the coherent measurement to noise limitations and echoes for photocurrents below and beyond the optimum, respectively. From the comparison of the BER curves versus photocurrent before the optimum point of photocurrent is reached, we can also remark that the slope of the BER curves reduces as data-rate increases. This indicates the presence of additional distortion or a more bandwidth-limited terahertz system.

Fig. 5(d) shows the BER at the respective optimum photocurrent as a function of the gross data rate. The highest spectral

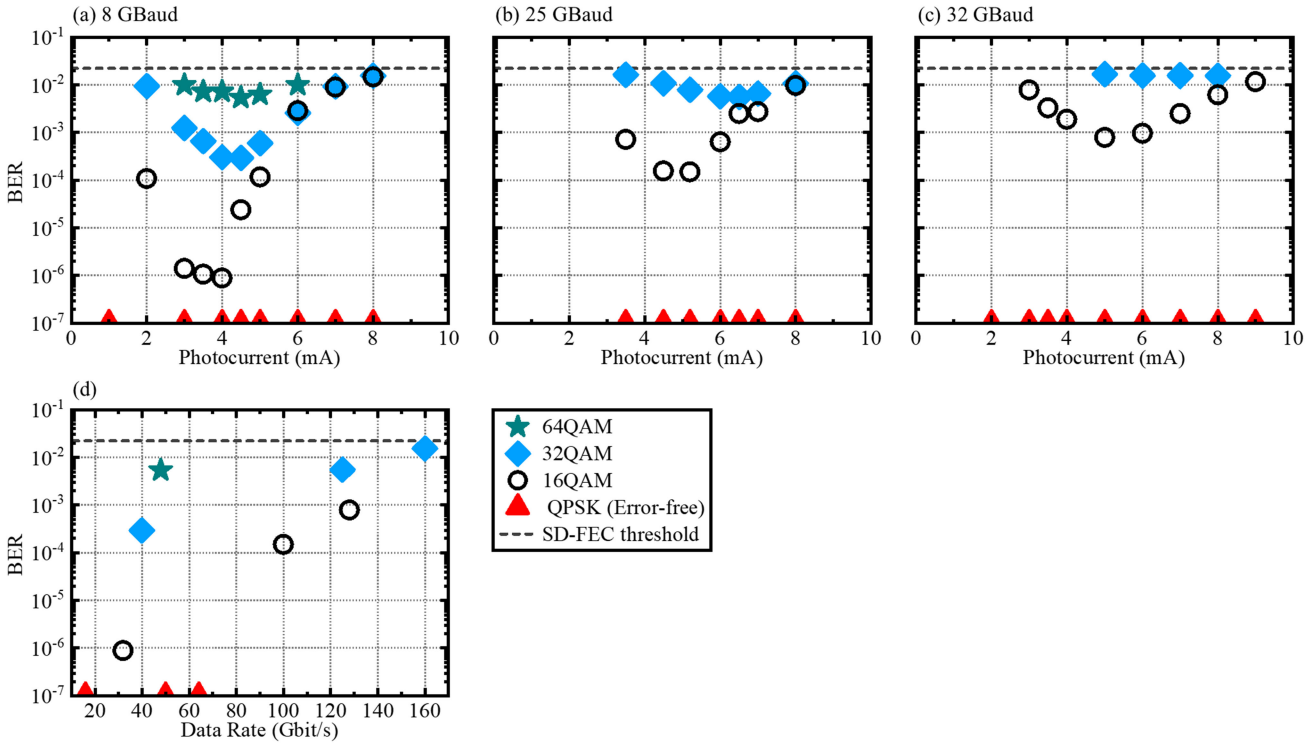

Fig. 5. The BER as a function of the photocurrent transmitted with the merged bowtie emitter for QPSK (red triangles), 16QAM (black circles), 32QAM (blue diamonds) and 64QAM (green stars) modulation. Symbol rates of 8 GBaud (a), 25 GBaud (b) and 32 GBaud (c) are shown. QPSK is error free for all symbol rates. For higher modulation formats, the BER reaches a minimum between 4 mA and 6.5 mA, whereas the optimal photocurrent increases with higher symbol rates. (d) Shows the BER as a function of the data rate at the respective best photocurrent. The grey dashed line indicates the threshold of 2.2×10^{-2} for soft-decision forward-error correction (SD-FEC) with 20% overhead.

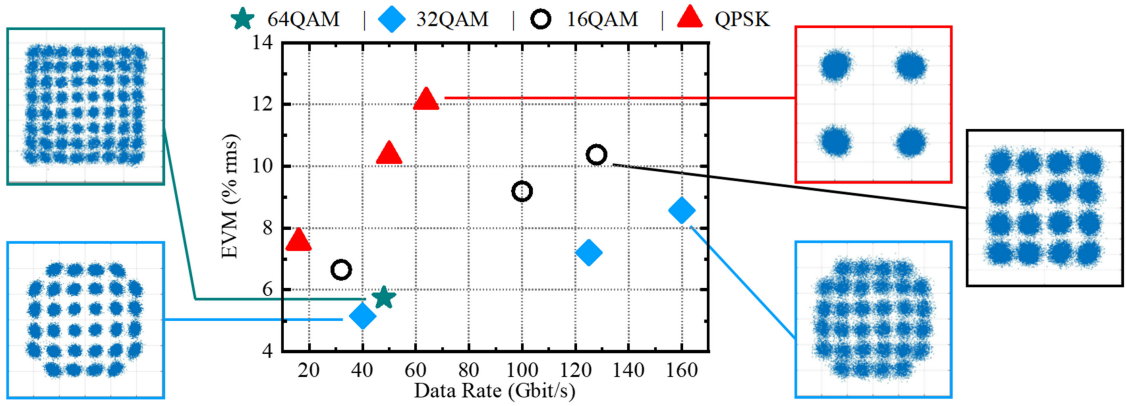

Fig. 6. The error vector magnitude (EVM) is shown as a function of data rate for the demonstrated modulation formats QPSK, 16QAM, 32QAM, and 64QAM. For all modulation formats, the EVM increases monotonically for increasing data rates. The constellation diagrams illustrate the evolution of the EVM.

efficiency is obtained with 64QAM at 48 Gbit/s line rate. In contrast, QPSK shows the lowest spectral efficiency. However, it can be transmitted even without SD-FEC and allows for 64 Gbit/s at 32 GBaud. With 16QAM, 128 Gbit/s gross data rate with a BER of 7.8×10^{-4} could be transmitted. The highest gross data rate of 160 Gbit/s is achieved with 32QAM modulation. Since the BER of 1.5×10^{-2} is still below the SD-FEC threshold with 20% overhead, this corresponds to 133 Gbit/s net data rate. To the best of our knowledge, this is the highest line rate for wireless 300 GHz link reported using a photodiode-based transmitter and the highest data rate at all using a PIN-PD transmitter. Even at 100 Gbit/s, which is the data-rate target of the new IEEE 802.15.3d standard, the signal integrity is still high with BER close to 10^{-4} [9].

In addition to the BER, the error vector magnitude (EVM) further indicates the quality of the terahertz transmission. Fig. 6 shows the EVM as a function of data rate for the employed modulation formats. The data points are the same as in Fig. 5(d). The strongest increase of EVM is observed for QPSK although the BER is quasi-zero for all symbol rates up to 32 GBaud.

Note the monotonic evolution of the EVM with the increase of data-rate indicating that the data link is free from resonances for theses bandwidths. The attached constellation diagram illustrate the progress of increasing EVM: although the EVM increases stronger than for 32QAM, QPSK and 16QAM modulation result in a clear and symmetric constellation diagram for the highest symbol rate of 32 GBaud, i.e., a data rate of 64 Gbit/s and 128 Gbit/s, respectively. Compared to that, the constellation diagram of 32QAM at 40 Gbit/s exhibits oval-shaped clusters at the outer symbols indicating higher impact of phase noise than amplitude noise. However, this behavior cannot be seen at 160 Gbit/s, where both phase and amplitude noise leads to increased EVM of more than 8 % rms. The constellation diagram for 64QAM at 48 Gbit/s shows more noise for the symbols at the corners, i.e., symbols with highest amplitude. However, the overall shape of the 64QAM constellation is quadratic with only slightly curved edges due to reduced amplitude for symbols close to the vertical Q-axis.

III. Conclusion

A 300 GHz wireless link was demonstrated using a photonic transmitter based on a PIN photodiode. Thanks to the photomixing approach, the data modulation could be done in the optical domain exploiting standard fiber-optical communication technology. On the receiver side, an amplified direct detector enabled the investigation of the NRZ-OOK link in real-time. For the coherent link, an electronic mixer was used to analyze data transmission with high spectral efficiency. First, two designs of antenna-integrated transmitters were investigated and compared in a 5 Gbit/s amplitude modulated link. Second, the most promising transmitter was characterized in a coherent link, and line rates up to 160 Gbit/s could be measured. In the first testbed, we observed a non-monotonic dependence of the bit-error-ratio (BER) on the optical input power, i.e., the photocurrent of the PD, for both transmitters. However, the antenna design influenced the BER as well. Moreover, the two transmitters reach their optimum performance at different photocurrent, respectively. Echoes in the eye diagrams indicate a poor signal integrity of one of the transmitters, which reduced the BER. The other antenna featured better signal integrity, i.e., less echoes, and allowed to measure a real-time BER of 7.5×10^{-13} for the 5 Gbit/s channel. In the coherent testbed, the QPSK signals were transmitted error-free enabling a 64 Gbit/s channel at 5 dBm optical input only. Here, that bandwidth was limited by the maximum symbol rate of our setup, which was 32 GBaud. For the highest spectral efficiency, we demonstrated 64QAM modulation at 8 GBaud resulting in 48 Gbit/s. The highest data rate was achieved with 32QAM at 32 GBaud. Here, 13 dBm optical power allowed for a BER of 1.5×10^{-2} which is still below the SD-FEC threshold assuming 20% overhead, i.e., 133 Gbit/s net data rate.

Our results proved the advantage of the photonic approach to enter the terahertz range for wireless communications: generation and amplification of the optical feed signal, modulation techniques, high-level modulation formats, and techniques for digital signal processing were adopted from mature fiber-optical communication. Moreover, the steady increasing toolbox of photonic integration promises even superior transmitters, e.g., with higher efficiency due to integrated amplifiers or increased stability due to integrated comb sources. On the terahertz side, however, the origin of the particular noise contribution and distortion requires further analysis. In combination with high frequency simulation of terahertz antennas, the experimental results are basis for a better understanding of the interplay between photodiode, antenna and substrate-integrated silicon lens. Thus, valuable guidelines for the design of photonic terahertz transmitters will be derived from the results reported in this work. Future antenna designs should focus on improved signal integrity and antenna gain in order to suit real-world communication scenarios, i.e., increased link distance and no need for optical elements in the free-space path.

References

[1] T. Nagatsuma, K. Oogimoto, Y. Inubushi, and J. Hirokawa, "Practical considerations of terahertz communications for short distance applications," *Nano Commun. Netw.*, vol. 10, pp. 1–12, 2016, doi: 10.1016/j.nancom.2016.07.005.

[2] W. Gerstacker and J. M. Jornet, "THz communications," *Nano Commun. Netw.*, vol. 10, pp. iv–iv, 2016, doi: 10.1016/S1878-7789(16)30071-0.

[3] H. Shams *et al.*, "100 Gb/s multicarrier THz wireless transmission system with high frequency stability based on a gain-switched laser comb source," in *IEEE Photon. J.*, vol. 7, no. 3, Jun. 2015, Art no. 7902011, doi: 10.1109/JPHOT.2015.2438437.

[4] I. Dan *et al.*, "300 GHz wireless link employing a photonic transmitter and active electronic receiver with a transmission bandwidth of 54 GHz," *IEEE Trans. Terahertz Sci. Technol.*, vol. 10, no. 3, pp. 271–281, Mar. 2020, doi: 10.1109/TTHZ.2020.2977331.

[5] C. Castro *et al.*, "32 GBd 16QAM wireless transmission in the 300 GHz band using a PIN diode for THz upconversion," in *Proc. Opt. Fiber Commun. Conf. Exhib.*, 2019, pp. M4F.5, doi: 10.1364/ofc.2019.m4f.5.

[6] T. Harter *et al.*, "Wireless THz link with optoelectronic transmitter and receiver," *Optica*, vol. 6, no. 8, pp. 1063–1070, 2019, doi: 10.1364/optica.6.001063.

[7] S. Jia, L. Li, Y. Fu, L. Oxenløwe, and H. Hu, "Integrated MLL chip-based PAM-4/DMT-16QAM photonic-wireless link in W-band for flexible applications," *Opt. Exp.*, vol. 29, no. 11, pp. 15969–15979, 2021, doi: 10.1364/oe.425314.

[8] T. Nagatsuma, G. Ducournau, and C. C. Renaud, "Advances in terahertz communications accelerated by photonics," *Nature Photon.*, vol. 10, no. 6, pp. 371–379, 2016, doi: 10.1038/nphoton.2016.65.

[9] IEEE, *IEEE Standard For High Data Rate Wireless Multi-Media Networks–Amendment 2: 100 Gb/S Wireless Switched Point-To-Point Physical Layer*, IEEE Std 802.15.3d-2017 (Amendment to IEEE Std 802.15.3-2016 as Amend. by IEEE Std 802.15.3e-2017), pp. 1–55, Oct. 2017, doi: 10.1109/IEEESTD.2017.8066476.

[10] T. Nagatsuma, H. Ito, and T. Ishibashi, "High-power RF photodiodes and their applications," *Laser Photon. Rev.*, vol. 3, no. 1–2, pp. 123–137, Feb. 2009, doi: 10.1002/lpor.200810024.

[11] J. L. Hesler, A. R. Kerr, W. Grammer, and E. Wollack, "Recommendations for waveguide interfaces to 1 THz," in *Proc. 18th Int. Symp. Space Terahertz Technol. 2007*, 2007, pp. 100–103. [Online]. Available: https://www.proceedings.com/05918.html

[12] Electronic Components Industry Association (ECIA), "EIA specification: Rectangular waveguides (WR3 to WR2300)," EIA-261-C (Revision RS-261-B) [Approved January 24, 2018], 2018.

[13] S. Nellen *et al.*, "Experimental comparison of UTC- and PIN-photodiodes for continuous-wave terahertz generation," *J. Infrared, Millimeter, Terahertz Waves*, vol. 41, no. 4, pp. 343–454, 2020, doi: 10.1007/s10762-019-00638-5.

[14] S. Nellen *et al.*, "Radiation pattern of planar optoelectronic antennas for broadband continuous-wave terahertz emission," *Opt. Exp.*, vol. 29, no. 6, pp. 8244–8257, 2021, doi: 10.1364/oe.416844.

[15] A. Morales, G. Nazarikov, S. Rommel, C. Okonkwo, and I. T. Monroy, "Highly tunable heterodyne sub-THz wireless link entirely based on optoelectronics," *IEEE Trans. Terahertz Sci. Technol.*, vol. 11, no. 3, pp. 261–268, Mar. 2021, doi: 10.1109/TTHZ.2021.3064188.

[16] J. Smith, M. Naftaly, S. Nellen, and B. Globisch, "Beam profile characterisation of an optoelectronic silicon lens-integrated PIN-PD emitter between 100 GHz and 1 THz," *Appl. Sci.*, vol. 11, no. 2, p. 465, 2021, doi: 10.3390/app11020465.
[17] R. Judaschke, M. Kehrt, and A. Steiger, "Comparison of waveguide and free-space power measurement in the millimeter-wave range," in *Proc. Int. Conf. Infrared, Millimeter, Terahertz Waves, IRMMW-THz*, Sep. 2019, pp. 1–2, doi: 10.1109/IRMMW-THz.2019.8874235.
[18] Analog Devices, "32 Gbps limitting amplifier," HMC866LC3 datasheet [v01.0614]. [Online]. Available: https://www.analog.com/media/en/technical-documentation/data-sheets/hmc866.pdf (accessed Oct. 21, 2021).
[19] Keysight Technologies, "PathWave vector signal analysis," 89600 VSA. [Online]. Available: https://www.keysight.com/de/de/products/software/pathwave-test-software/89600-vsa-software.html (accessed Oct. 20, 2021).
[20] S. Preu, G. H. Döhler, S. Malzer, L. J. Wang, and A. C. Gossard, "Tunable, continuous-wave terahertz photomixer sources and applications," *J. Appl. Phys.*, vol. 109, no. 6, 2011, Art. no. 061301, doi: 10.1063/1.3552291.

Simon Nellen received the B.S. and M.S. degrees in physics from the Technical University of Berlin, Berlin, Germany, in 2012 and 2015, respectively. He is currently working toward the Ph.D. degree in physics with Fraunhofer Heinrich Hertz Institute (HHI), Berlin, Germany.

From 2012 to 2015, he was a Student Research Assistant with Terahertz Sensor Systems Group, Fraunhofer HHI. At this time, he investigated ultrafast photoconductive switches for pulsed terahertz generation and detection for his master thesis. Afterwards, he joined Fraunhofer HHI as a Research Associate. He is the author of more than 60 publications in peer-reviewed international journals or peer-reviewed conferences proceedings, and two inventions. His research interests include photonic devices for continuous wave terahertz generation and detection, monolithically integrated antennas and radio frequency structures, sensing and communication at terahertz frequencies, and photonic integrated circuits for those applications.

Sebastian Lauck received the B.S. and M.S. degrees in electrical engineering from the Technical University of Berlin, Berlin, Germany, in 2017 and 2019, respectively. He is currently a Research Associate with Fraunhofer Heinrich Hertz Institute (HHI), Berlin, Germany.

From 2016 to 2019, he was a Student Research Assistant with Terahertz Sensor Systems Group, Fraunhofer HHI. At this time, he investigated photodiode based antenna structures for photonic integrated terahertz emitter for his master thesis. Afterwards, he joined Fraunhofer HHI as a Research Associate as a RF Engineer for photonic integrated circuits and antennas. His research interests include photonic devices for continuous wave terahertz generation and detection, RF and optical packaging of monolithically integrated modulators, design and simulation of broadband terahertz antennas for sensing, and communication.

Emilien Peytavit received the Engineering degree from the Ecole Centrale de Lille, Villeneuve-d'Ascq, France, in 1999, and the Ph.D. degree in electrical engineering from the University of Lille, Lille, France, in 2002, working on terahertz generation by optical heterodyne techniques, also called photomixing.

From 2003 to 2005, he was a Postdoctoral Researcher with CEA-Leti, Grenoble, France, working on microbolometer arrays for terahertz detection. Since 2005, he has been a CNRS Research Scientist with the Institute of Electronics, Microelectronics and Nanotechnology, University of Lille. He is the author or co-author of more than 50 journal papers, 100 international conference papers, and three patents. His research interests include the generation and detection of THz waves by using photonics-based-techniques.

Pascal Szriftgiser (Senior Member, IEEE) received the Ph.D. degree in quantum physics from Laboratoire Kastler Brossel, University Paris VI, Paris, France, in 1996. He then joined the Laboratory Physique des Lasers Atomes et Molécules (PhLAM), as a CNRS Researcher. Since 2012, he has been the CNRS Research Director, Leader of the Cold Atoms Group, and the Deputy Director of the Laboratory PhLAM. He is the co-author of 77 publications in peer-reviewed journals. His expertise spans from cold atoms physics and quantum chaos, non-linear optics in optical fibers to high-speed optical coherent communications for THz applications.

Martin Schell (Member, IEEE) received the Diploma in physics from RWTH Aachen University, Aachen, Germany, in 1989, and the Dr.rer.nat. degree from the Technical University of Berlin, Berlin, Germany, in 1993. In 1995, he was Visiting Researcher with the University of Tokyo, Tokyo, Japan. From 1996 to 2000, he was Management Consultant with The Boston Consulting Group. From 2000 to 2005, he was a Product Line Manager, and then the Head of Production and Procurement, Infineon Fiber Optics, Berlin, Germany. He is currently the Director of the Fraunhofer Heinrich Hertz Institute, Berlin and a Professor of optic and optoelectronic integration with the Technical University of Berlin. From 2015 to 2021, he was a Board Member of the European Photonics Industry Consortium. He currently is the Chairman of the Competence Network Optical Technologies Berlin/Brandenburg (OptecBB), spokesman of the Berlin-Brandenburg Photonics Cluster, and a Member of the Photonics21 Board of Stakeholders.

Guillaume Ducournau (Member, IEEE) received the master's degree from Rouen University, Mont-Saint-Aignan, France, in 2002, and the Ph.D. degree from the Université de Rouen, Rouen, France, working on fiber optic communication systems using DPSK/DQPSK in 2005.

He is currently a Full Professor with the Institute of Electronics, Microelectronics and Nanotechnology (IEMN)/University of Lille and Polytech'Lille Graduate School, THz Photonics Group. He is the Leader of the THz wireless communications activity with IEMN using optoelectronic THz photomixers, electronic receivers, THz instrumentation, and mm-wave characterization. He is the author or co-author of more than 180 publications in peer-reviewed international journals or peer-reviewed conferences proceedings and holds a patent. He coordinated the ANR/DFG TERASONIC Project for the use of THz photonics technologies and electrical solid-state technologies for 100 Gbps wireless links. He actually coordinates the ANR-DFG SOLITONIC project also for THz communications in the 300 GHz band. He is also a Member of the ThoR Project, an EU-Japan funded project for the development super-heterodyne THz transmission systems using IEEE 802.15.3 d standard.

He is a Member of the IEEE MTT-21 Terahertz Technology and Applications Committee.

Björn Globisch studied physics in Aachen, Madrid and Berlin, Germany. He received the Diploma in physics from the Technical University of Berlin, Berlin, Germany, in 2011, and the Ph.D. degree in physics from the Philipps University Marburg, Germany, in 2017. Afterwards, he joined Fraunhofer Heinrich Hertz Institute (HHI) as a Research Associate. Since 2017, he has been the Head of Terahertz Sensor Systems Group, Fraunhofer HHI and since 2019, he has also been an Associate Professor of terahertz sensing with the Institute of Solid State Physics, Technical University of Berlin. He is the author of one book chapter, more than 40 articles, and six inventions. His research interests include transport and ultrafast phenomena in semiconductors, pulsed and continuous wave terahertz components and systems as well photonic integrated circuite for terahertz generation and detection.